J Porous Mater (2012) 19:95–102
DOI 10.1007/s10934-011-9452-2

α-Amylase immobilization capacities of mesoporous silicas with different morphologies and surface properties

Kanako Hisamatsu · Toru Shiomi · Shun-ichi Matsuura · Takayuki Y. Nara · Tatsuo Tsunoda · Fujio Mizukami · Kengo Sakaguchi

Published online: 29 January 2011

Abstract α-Amylase was encapsulated in several mesoporous materials (folded sheet mesoporous silica (FSM), cubic mesoporous silica (KIT-6), and two-dimensional hexagonal mesoporous silica (SBA-15)) that differed morphologically in terms of particle shape, pore size, and pore structure. The encapsulation capacity and thermal stability of encapsulated α-amylase were examined. The amount of α-amylase encapsulated increased with increasing pore size in the following order: SBA-15 < KIT-6 < FSM. Nitrogen adsorption experiments were performed before and after α-amylase encapsulation in mesoporous silicas with pore sizes larger than the size of α-amylase, confirming that α-amylase was encapsulated in the pores. Among mesoporous silicas with similar pore sizes, FSM was found to have the highest capacity for α-amylase encapsulation both per weight and per surface area of silica. Furthermore, α-amylase encapsulated in FSM demonstrated high thermal stability at 90 °C relative to the thermal stability of free α-amylase or free α-amylase encapsulated in other mesoporous silicas. Zeta potential measurements showed that the FSM surface had an isoelectric point that was lower than that of other mesoporous silicas, and hydrophilicity measurements showed that its surface was more hydrophilic. The surface properties of FSM contributed to the high thermal stability of the α-amylase encapsulated within the pores.

Keywords Mesoporous silica · Protein encapsulation · Immobilized enzyme · α-amylase

K. Hisamatsu · K. Sakaguchi
Department of Applied Biological Science, Tokyo University of Science, Faculty of Science and Technology, Science University of Tokyo, 2641 Yamazaki, Noda, Chiba 279-8510, Japan

T. Shiomi · S. Matsuura · T. Y. Nara · T. Tsunoda (✉) · F. Mizukami
Research Center for Compact Chemical Process, National Institute of Advanced Industrial Science and Technology (AIST), Central 5, 1-1-1 Higashi, Tsukuba-shi, Ibaraki-ken 305-8565, Japan
e-mail: t.tsunoda@aist.go.jp

1 Introduction

Enzymes immobilized on supports are of considerable interest for use in enzyme reactors, biological fuel cells, and biosensors [1]. Among the various support materials tested, mesoporous silica has been an attractive enzyme encapsulation support candidate since its discovery [2, 3] due to its tenability over a wide range of pore size, from 2 to 50 nm, a relatively large surface area, and a high fraction of total pore volume [4, 5]. These structural characteristics convey a large enzyme loading capacity that yields a high density of active enzymes. Because the pore size, pore structure, and particle morphology may be controlled, the support structure may be altered to accommodate specific enzymes. Thus far, enzyme encapsulation has been achieved using several types of mesoporous silicas, including SBA-15, MCM-41, PMO, and FSM [6–10].

Different mesoporous silica materials display a variety of encapsulation properties and enzymatic activities. For example, Takahashi et al. [11] reported that FSM-16 and MCM-41 materials adsorbed larger amounts of horseradish peroxidase, which yielded higher enzymatic activities per adsorbed enzyme, than did SBA-15 materials. The catalytic activity of acetylcholinesterase was higher when encapsulated in FSM than in MCM, even though both materials showed similar immobilization capacities [12]. An oligomeric hemoglobin, encapsulated in FSM mesopores with

tuned pore sizes, was report to have been protected from denaturation and aggregation induced by heat, high ionic strength, or chemically harsh conditions [13].

The development of mesoporous silica as an immobilization support can be advanced by characterizing the factors that affect the encapsulation behavior of enzymes within mesoporous silica, such as the pore size, pore structure, and surface characteristics. The physicochemical properties of the support material affect both enzyme immobilization and basic biochemical activity. In particular, hydrophilic properties, van der Waals interactions, and electrostatic attractive forces are key factors for the control of enzyme adsorption, as well as contributing to the retention of enzymatic activity [14]. If the interaction between an enzyme and the silica surface is too weak, the enzyme may escape from the encapsulation matrix. If the interaction is too strong, the immobilized enzyme may gradually change conformation, resulting in decreased enzymatic activity [15].

In this work, we prepared three types of mesoporous silica (FSM, KIT-6, and SBA-15) with different pore size, pore structure, and morphology. The silica substrates were characterized by scanning electron microscopy (SEM), transmission electron microscopy (TEM), X-ray diffraction (XRD), and nitrogen adsorption/desorption measurements. Using these mesoporous silicas as supports, with α-amylase as a model enzyme, we investigated the adsorption capacity of the materials for α-amylase. The morphological properties that affected the adsorption capacity were evaluated. The effects of the surface characteristics and morphological properties on the thermal stability of the encapsulated α-amylase enzymes were also discussed.

2 Experimental

2.1 Materials

Docosyltrimethylammonium chloride ($C_{22}H_{45}N(CH_3)_3Cl$; C_{22}–TMA) and Kanemite (layered polysilicate) were kindly donated by Lion Corporation (Tokyo, Japan) and Tokuyama Siltech (Yamaguchi, Japan), respectively. 1,3,5-Toriisopropylbenzene (TIPB) was purchased from Tokyo Chemical Industry (Tokyo, Japan). α-Amylase from *Bacillus licheniformis* and a triblock copolymer ($EO_{20}PO_{70}EO_{20}$, Pluronic P123) were purchased from Sigma–Aldrich, Japan KK (Tokyo, Japan). Water-soluble starch and all other analytical grade reagents were obtained from WAKO Pure Chemical Industries Ltd. (Osaka, Japan).

2.2 Preparation of FSMs

FSM was synthesized as described by Urabe et al. [13]. In brief, for the preparation of FSM-4.0, kanemite (5.33 g) was dispersed in an aqueous solution (105 mL) and stirred at 70 °C for 30 min. The mixture was subsequently added to the C_{22}–TMA (10.0 g) solution in 100 mL H_2O and stirred vigorously at 70 °C for 2 h. The suspension was adjusted to pH 8.5 with 2 N HCl, stirred for 40 min, then incubated for a further 3 h at 70 °C. For the synthesis of FSM with pore sizes of 7.5 or 9 nm (FSM-7.5 or FSM-9.0), 7.5 or 15 g of the swelling reagent (TIPB), respectively, were stirred in the C_{22}–TMA solution for 30 min prior to the addition of kanemite. The resulting product was washed with deionized water (70 °C), dried overnight at 60 °C, and calcined at 550 °C in air for 6 h to remove organic compounds.

2.3 Preparation of SBA-15s

SBA-15 two-dimensional (2D) hexagonal mesoporous silicas were prepared using TEOS as the silica source and the triblock copolymer (P123: $EO_{20}PO_{70}EO_{20}$) as the template, in accordance with the method reported by Zhao et al. [16] with slight modification. SBA-15 with a pore size of 6.1 (SBA-15-6.1) was synthesized as follows: 12 g P123 was dissolved in 449 mL H_2O, and 20 mL 35% HCl was added. After stirring the solution to completely disperse P123 at 35 °C, 27.4 mL TEOS was added and the solution was vigorously stirred by aging at 35 °C for 20 h. Subsequently, the reaction solution was transferred to a Teflon vessel and aging was carried out at 35 °C for 24 h in static conditions. Aging temperatures for SBA-15-9.9 and SBA-15-11 were 100 and 130 °C, respectively. The solid product was recovered by filtration, washed with ddH_2O, then dried at 60 °C. Calcinations of dried samples were carried out at 550 °C for 12 h under a constant airflow.

2.4 Preparation of KIT-6s

KIT-6 cubic mesoporous silicas were prepared according to the method reported by Freddy et al. [17]. KIT-6 samples, with pore sizes of 6.2, 8.0, or 11.1 nm (KIT-6-6.2, KIT-6-8.0, or KIT-6-11, respectively), were synthesized by aging at 35, 100, or 130 °C, respectively. The solid products were recovered by filtration, washed with ddH_2O, and dried at 60 °C. Calcinations were carried out at 550 °C for 12 h under a constant airflow.

2.5 Characterization

Nitrogen adsorption/desorption isotherms were obtained using a NOVA 3000 analyzer (Quantachrome Instruments, FL, USA) at liquid nitrogen temperature. Prior to measurement, the samples were degassed at 120 °C for 3 h (before loading) and at 60 °C for 24 h (after loading α-amylase). Specific surface areas were calculated by the

Brunauer–Emmett–Teller (BET) method using adsorption data from $P/P_0 = 0.05$ to $P/P_0 = 0.30$. Pore size distributions were determined by analyzing the adsorption branch using the Barrett–Joyner–Halenda (BJH) method. TEM analysis was performed on a JEM-2010F microscope (JEOL Ltd, Tokyo, Japan) operated at 200 kV. SEM images were obtained using an S-800 microscope (Hitachi High-Technologies Corporation, Tokyo, Japan) operated at 10 kV. Powder XRD patterns were recorded using an MXP-3TZ powder X-ray diffractometer (Bruker AXS KK, Kanagawa, Japan) equipped with Cu Kα radiation (40 kV, 55 mA) over the range 0.5–5.0°. Zeta potentials were measured using an ELS-Z (Otsuka Electronics Co. Ltd.) with 10 mg mL^{-1} silica solutions of varying pH (2.0–10.0). The water adsorption capacities of the mesoporous silicas were measured using a BELSORP-18 instrument (BEL Japan, Inc. Osaka, Japan).

2.6 Encapsulation of α-amylase in the various mesoporous silicas

Ten milligrams of mesoporous silica were incubated with 1 mL α-amylase solution (1–20 mg mL^{-1}) at 4 °C for 3 h on a rotator RT-50 (Taitec Corporation, Saitama, Japan) to establish the adsorption equilibrium. Encapsulated α-amylase was collected by centrifugation at 20,800 $\times g$ for 5 min at 4 °C. The amount of encapsulated α-amylase was determined by subtracting the amount of protein in the supernatant after centrifugation from the amount of α-amylase present before adsorption. The mesoporous silicas containing encapsulated α-amylase (α-amylase–silica conjugate) were used in subsequent enzymatic activity assays.

2.7 α-Amylase assay

α-Amylase activity was measured by determining the quantity of starch remaining after reaction. Enzyme activity was measured as follows. Ten milligrams of α-amylase–silica conjugatewere dispersed in 1 mL 50 mM MOPS buffer (pH 7.0). Ten microliters of α-amylase–silica conjugate were then mixed with 0.50 mL starch solution in 50 mM buffer (pH 7.0) and incubated at 37 °C for 7.5 min with shaking. The mixture was subsequently centrifuged at 20,800 $\times g$ for 5 min at 4 °C to remove α-amylase–silica conjugates, and the quantity of starch remaining in the supernatant was determined using the iodo–starch reaction. Five milliliters of the reaction mixture were transferred to a 96-well titer plate, and 190 μL H_2O and 5 μL 0.01 M KI were added. The absorbance at 660 nm was measured to determine the quantity of remaining starch by staining with KI. The activity unit was defined in terms of the amount of starch that was hydrolyzed by 0.5 mg α-amylase in 7.5 min.

2.8 Thermal stability of α-amylase encapsulated in mesoporous silica

An aliquot of mesoporous silica was incubated with 1 mL α-amylase solution (0.5 mg mL^{-1}) to establish the adsorption equilibrium. The mixture was centrifuged at 20,800 $\times g$ for 5 min at 4 °C to remove the supernatant. Next, the mixture was added to 1 mL 50 mM MOPS buffer (pH 7.0), and was heated at 90 °C for 5, 10, 20, 30, 40, 50, or 60 min. In the case of free α-amylase, 0.5 mL of the free enzyme (0.50 mg mL^{-1}) in 50 mM MOPS buffer (pH 7.0) was heated at 90 °C for 5, 10, 20, 30, 40, 50, or 60 min. The enzyme activity was then measured as described above.

3 Results and discussion

3.1 Characterization of the morphologies of the mesoporous silicas

Figure 1 shows SEM and TEM images of each type of mesoporous silica. FSM and KIT-6 displayed random amorphous morphologies without defined particle shapes (Fig. 1a, b), whereas SBA-15 displayed a long agglomerated rod-shaped morphology composed of 800 nm diameter rods (Fig. 1c). TEM showed that KIT-6 featured ordered three-dimensional (3D) mesoporous structures consisting of randomly oriented domains (Fig. 1e) and that SBA-15 featured well-ordered 2D channel structures (Fig. 1d). A 2D ordered mesoporous structure similar to that of SBA-15 was also observed in FSM-4.0 (data not shown). In contrast, FSM-7.5 and FSM-9.0 featured disordered but highly mesoporous structures with relatively thin walls, as shown in Fig. 1d.

These morphological features were confirmed by XRD (Fig. 2). The well-resolved peaks of SBA-15 ($2\theta = 0.86°$, 1.56°, and 1.80°) and FSM-4.0 ($2\theta = 1.79°$, 3.06°, and 5.40°) were associated with a 2D hexagonal p6 mm structure [16], and the peak pattern of KIT-6 corresponded to a cubic Ia3d structure [17]. Unlike these well-ordered materials, FSM-7.5 and FSM-9.0 exhibited only broad patterns with a single main peak (at $2\theta = 1.06°$ and 1.08°, respectively) indexed to a (100) structure and a second broad peak at $2\theta = 2°$. These corresponds to a disordered arrangement of pores, that is, the absence of long range channels as observed by TEM (Fig. 1d), indicating the mesocellular foam type structure of FSM-7.5 and FSM-9.0.

The mesoporous features of FSM, KIT-6, and SBA-15 were evaluated by nitrogen adsorption/desorption isotherms (Fig. 3, Table 1). All materials showed type IV isotherms, classified according to the International Union of Pure and Applied Chemistry (IUPAC) classification scheme, which

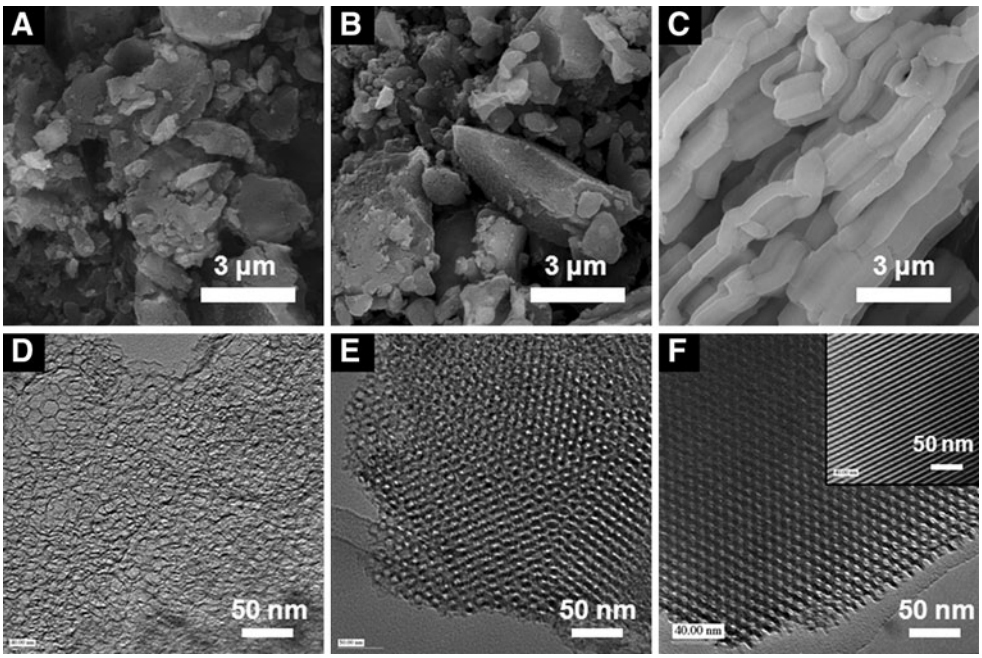

Fig. 1 SEM and TEM images of **a**, **d** FSM-9.0; **b**, **e** KIT-6-11; and **c**, **f** SBA-15-11

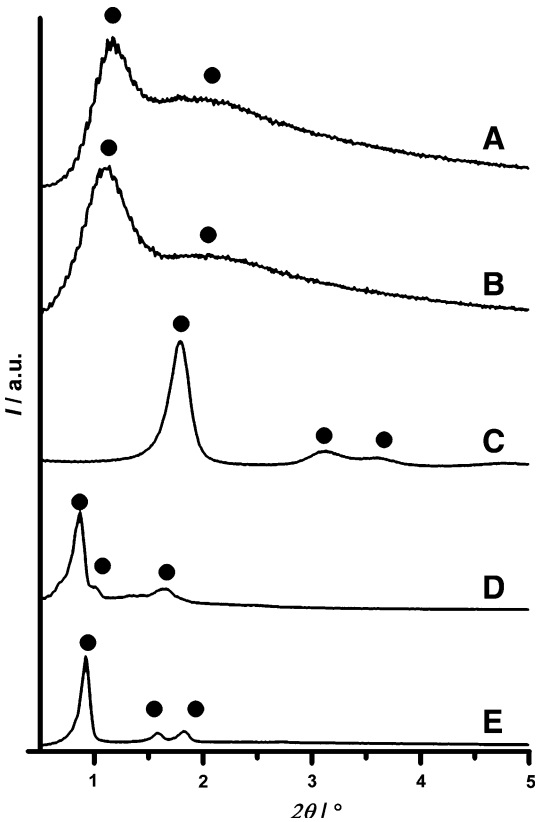

Fig. 2 Low-angle XRD patterns of mesoporous silica. (*A*) FSM-9.0, (*B*) FSM-7.5, (*C*) FSM-4.0, (*D*) KIT-6-11, and (*E*) SBA-15-11

were characteristic of mesoporous materials [18]. All KIT-6s and SBA-15s (synthesized at different aging temperatures) exhibited similar isotherm patterns and narrow pore size distributions, and the only difference between materials was the pore size. The pore size distributions of the FSMs (except for FSM-4.0) were relatively broad, and the mesopore size was distributed over tens of nanometers to produce a higher total pore volume and BET surface than was observed in the KIT or SBA materials, which are well consistent with the presented mesocellular foam type structure of FSM-7.5 and -9.0 by TEM and XRD.

3.2 Encapsulation of α-amylase in the various mesoporous silicas

The α-amylase adsorption capacities of the mesoporous silicas were calculated from the adsorption equilibria (Table 1). Among mesoporous silicas of a given type, the adsorption capacities increased with increasing pore size and total pore volume, even though the surface area remained constant across samples. Among the FSMs, α-amylase adsorbed only slightly onto FSM-4.0, which had a pore size that was much smaller than the size of α-amylase (dimensions: 4.5 × 5.1 × 8.5 nm). In contrast, FSM-7.5 and FSM-9.0, which had pore sizes larger than the size of α-amylase, showed a high capacity for loading α-amylase. The adsorption capacities of KIT-6 and SBA-15 also increased with increasing pore size. Most of the surface area in mesoporous silicas is contributed by the inner pore surfaces of the mesoporous structure. Therefore, these results indicate that the ability of the pore surface to adsorb α-amylase in a mesoporous material depended on size matching between the pore and the α-amylase molecule.

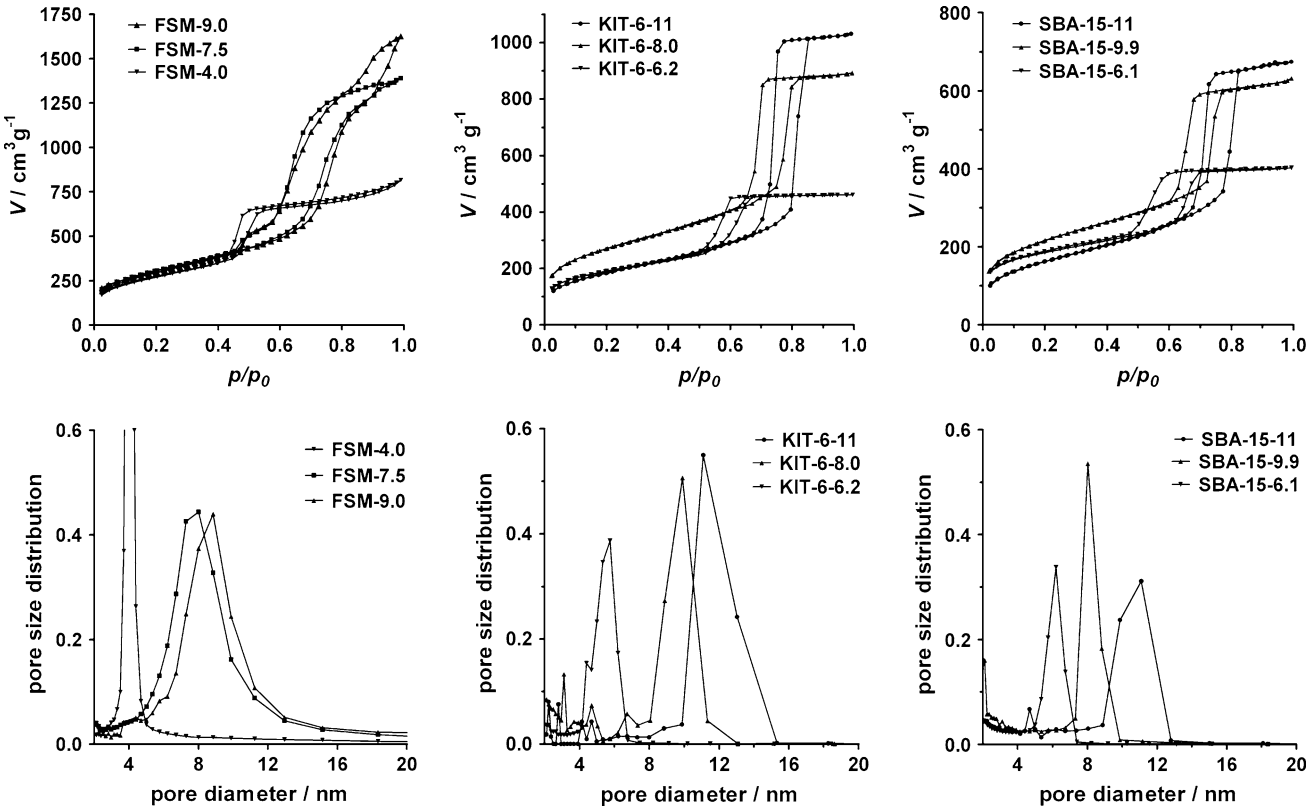

Fig. 3 Nitrogen adsorption–desorption isotherms and pore size distributions of mesoporous silicas

Table 1 Physicochemical properties and α-amylase encapsulation properties of the mesoporous silicas

Sample	Pore size [nm]	BET surface area [m^2 g^{-1}]	Total pore volume [cm^3 g^{-1}]	Adsorption capacity[a] [mg g^{-1} of silica]	Adsorption capacity[b] [mg m^{-2} of silica]
FSM-4.0	4.0	969	1.30	55	0.057
FSM-7.5	7.5	950	2.10	279	0.294
FSM-9.0	9.0	1,070	2.50	555	0.519
KIT-6-6.2	6.2	648	0.71	61	0.094
KIT-6-8.0	8.0	934	1.38	131	0.140
KIT-6-11	11.1	670	1.59	172	0.257
SBA-15-6.1	6.1	633	0.62	45	0.070
SBA-15-9.9	9.9	760	0.98	82	0.108
SBA-15-11	11.0	635	1.04	138	0.217

[a] Defined as the maximum amount of α-amylase encapsulated per 1 g silica

[b] Defined as the maximum amount of α-amylase encapsulated per 1 m^2 silica, which was calculated from the N_2 BET surface area

A comparison between FSM, KIT-6, and SBA-15 showed that FSM-9.0 had the highest adsorption capacity per 1 g silica. Although all three mesoporous silicas had pores that were large enough to encapsulate α-amylase, FSM-9.0 showed twice the adsorption capacity per unit surface area of either KIT-6-11 or SBA-15-11. To confirm whether α-amylase was entirely encapsulated within the pores, nitrogen adsorption/desorption analysis was performed on a set of mesoporous silicas with a given pore size both before and after α-amylase loading. As shown in Fig. 4, nitrogen adsorption in all three mesoporous silicas was dramatically reduced after α-amylase was loaded, suggesting that α-amylase was encapsulated within the pores. The peak of the pore size distribution of FSM-9.0 not only decreased in height after α-amylase encapsulation but also shifted to a smaller diameter (Fig. 4a inset). These

results indicated that the pores of FSM-9.0 were occupied by α-amylase. In contrast, the peak height of the pore size distributions did not decrease for either KIT-6-8.0 or SBA-15-9.9 (Fig. 4b, c). These results indicate different localization properties of α-amylase in the mesopores of these materials.

The number of pore entrances within a particle of the material increased with decreasing particle size, leading to improved encapsulation of the enzymes [19]. As shown in Fig. 1, the ordered straight channel structure of SBA-15 contained fewer entrances than did KIT-6 or FSM. Fewer entrances appeared to decrease the rate of diffusion of α-amylase into the deep inner ports of the particles, resulting in the localization of encapsulated α-amylase at the mesopores positioned closest to the entrances. The disordered pore arrangement and the presence of larger pores distributed across a length scale of tens of nanometers in the FSM particles favored more efficient adsorption relative to the well-ordered pores of KIT-6.

3.3 Enzyme activity and thermal stability of encapsulated α-amylase

α-Amylase is a glycogenase (EC number 3.2.1.1) that catalyzes the endohydrolysis of 1,4-α-D-glycosidic linkages in polysaccharides containing three or more 1,4-α-linked glucose units [20]. To evaluate the encapsulated state of α-amylase within the mesopores, we carried out enzymatic activity assays using starch as the substrate. The specific activities of α-amylase encapsulated in FSM-7.5 and FSM-9.0 were 0.59 and 0.60 unit mg^{-1}, respectively. FSM-4.0 showed a low specific activity of 0.03 unit mg^{-1} due to the leaching of α-amylase. KIT-6-11 and SBA-15-11 yielded activities of 0.23 and 0.38 unit mg^{-1}. These results suggest that the enzymatic activity and, therefore, the conformation of α-amylase appeared to be better conserved in FSM than in KIT-6 or SBA-15. The specific activity of α-amylase in MCF types of mesoporous silica was previously observed to be higher than in MCM-41 or SBA-15 materials [21]. Although the silica sources and synthesis conditions differed among the three materials, FSM-7.5, FSM-9.0, and MCF showed similar morphological features, such as pore size distribution and disordered pore arrangement. These features may have contributed to the higher specific activity of encapsulated α-amylase.

To ascertain whether FSM had a stabilizing effect on the encapsulated α-amylase, changes in specific activity were observed as a function of the duration of heat treatment at 90 °C prior to the enzyme activity assay (Fig. 5). α-Amylase encapsulated in FSM-7.5 and FSM-9.0 retained over 70% enzyme activity, even after a 60 min heat treatment, whereas α-amylase encapsulated in SBA lost almost all activity after 10 min heat treatment, similar to the activity loss observed in free α-amylase. FSM enhanced the stability of α-amylase within its pores if the appropriate pore size was provided.

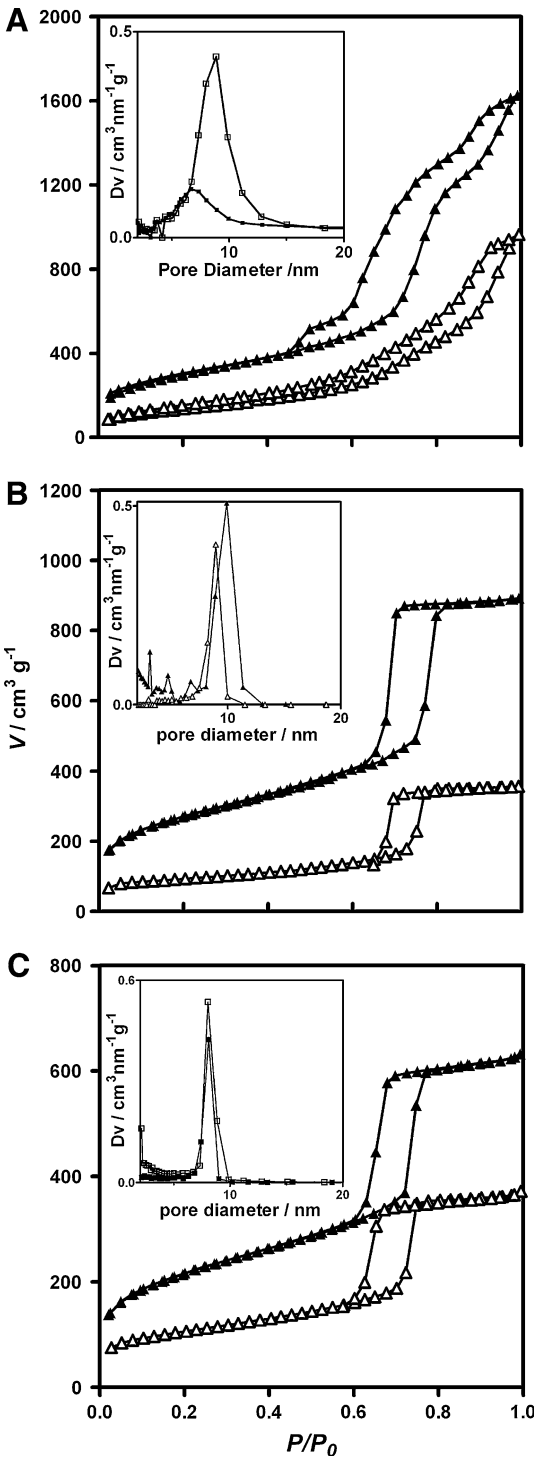

Fig. 4 Changes in nitrogen adsorption–desorption isotherms and corresponding pore size distribution curves from the adsorption branch before (*filled triangle*) and after (*open triangle*) loading α-amylase into the following mesoporous silicas: **a** FSM-9.0, **b** KIT-6-8.0, and **c** SBA-15-9.9

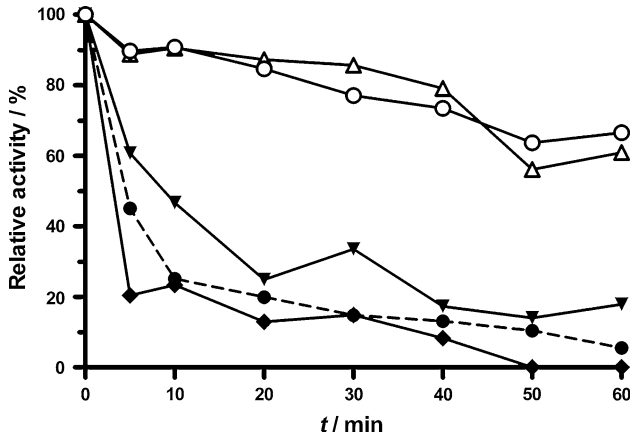

Fig. 5 Thermal stability of α-amylase encapsulated in mesoporous silicas: FSM-9.0 (*open circle*), FSM-7.5 (*open triangle*), SBA-15-11 (*filled inverted triangle*), KIT-6-11 (*filled diamond*), and the free enzyme (*filled circle*). The relative enzymatic activity was calculated with respect to the specific activity measured without heat treatment (defined as 100%)

3.4 Surface properties of the mesoporous silicas

The isoelectric point (pI) of α-amylase is 6.7, so that it is positively charged in the enzyme assay solution (pH 7.0). At this pH, the silanol groups of mesoporous silicas were negatively charged, so that the silica surface and α-amylase interacted electrostatically. In fact, the adsorption of α-amylase was most efficient at pH values below 7.5. In addition to the electrostatic potential, the hydration level of the environment surrounding a protein is important for the stability of the protein [22]. Therefore, we investigated the surface properties of mesoporous silicas, the zeta potential and the hydrophilic ratio, to explore why α-amylase encapsulated in FSM was the only system to show thermal stability.

Figure 6 shows the zeta potentials of the mesoporous silicas at pH 2–10, showing that the pI of FSM was lower than that of KIT-6 or SBA-15. This result agreed well with a previous report that described the silanol surface groups of FSM as being more acidic than those of silica gel [23]. Table 2 shows the hydrophilic ratio of mesoporous silicas estimated from the ratio of BET surface areas determined from water adsorption and N_2 adsorption isotherms. The hydrophilic ratios of FSM-7.5 and FSM-9 were higher than those of KIT-6-11 or SBA-15-11. The difference in hydrophilicity is thought to have arisen from the silica source and the mechanism of the material's formation. TEOS was used to synthesize SBA-15 and KIT-6. TEOS is hydrolyzed under an acid catalyst and has been shown to form a high-density 3D network of siloxane polymers, observed (by TEM) to form a thick pore wall because all silanol groups of $Si(OH)_4$ cooperated in self-assembly [24]. In contrast, the kanemite framework used as the silica source for FSM consisted almost entirely of Q^3 silicate species [25]. Kanemite is hydrolyzed at pH 11.5 and is condensed at pH 8.5 by slow adjustments to the pH. As a result, FSM may have retained more silanol groups than did KIT-6 or SBA-15. The hydrophilicity of the silica was strongly influenced by the density of the surface silanol groups. These silanol groups probably improved hydration

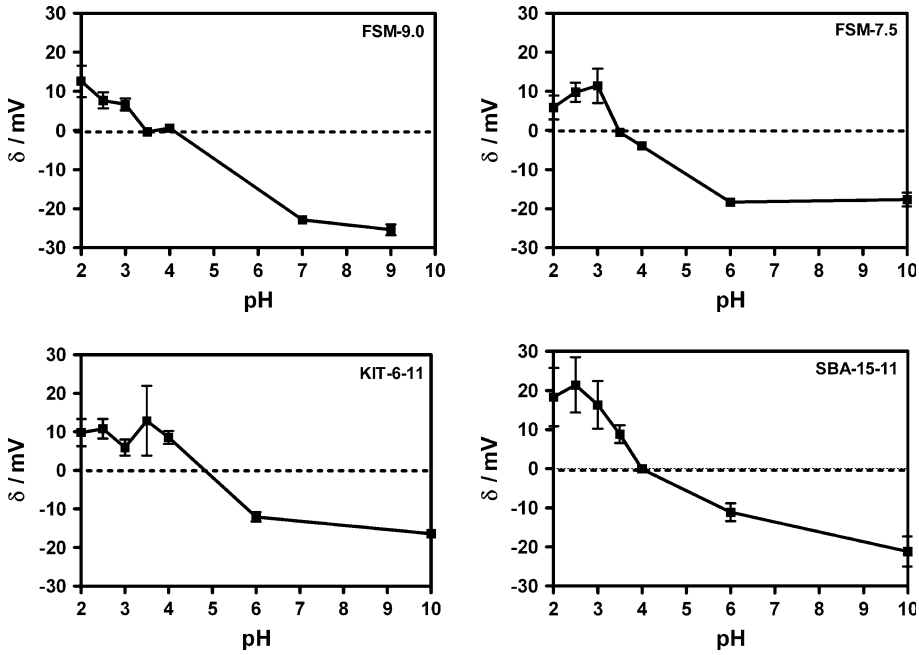

Fig. 6 Zeta potential of the mesoporous silicas

Table 2 Hydrophilic ratio of the mesoporous silicas

Sample	H_2O BET surface area A_{water} [$m^2\ g^{-1}$]	N_2 BET surface area $A_{nitrogen}$ [$m^2\ g^{-1}$]	Ratio [$A_{water}/A_{nitrogen}$]
FSM-7.5	198	950	0.21
FSM-9.0	183	1,070	0.17
KIT-6-11	85	635	0.13
SBA-15-11	98	670	0.14

of the proteins in the narrow silica pores, leading to added stability of the encapsulated α-amylase enzymes.

4 Conclusions

In conclusion, we measured the α-amylase adsorption capacities of several mesoporous silicas (FSM, KIT-6, and SBA-15) and evaluated the activities and thermal stabilities of the encapsulated enzymes. Mesoporous structures with pore sizes larger than the diameter of α-amylase were shown to be essential for the encapsulation of α-amylase within the pores. Compared with KIT-6 and SBA-15, FSM demonstrated the highest adsorption capacity due to its morphological characteristics: smaller particle size and the presence of larger pores with a disordered arrangement that provided more entrances per particle to enhance the enzyme diffusion efficiency. Furthermore, α-amylase encapsulated within FSM-7.5 or FSM-9.0 exhibited enhanced thermal stability. The enzyme stability was investigated by measuring the surface properties of the mesoporous silicas. The hydrophilicity ratio was suggested to play a key role in stabilizing the encapsulated α-amylase. These findings suggest improvements for the design of mesoscale structures for biomolecule immobilization.

References

1. W. Aehle, *Enzymes in Industry: Production and Applications* (Wiley-VCH, New York, 2007)
2. C.T. Kresge, M.E. Leonowicz, W.J. Roth, J.C. Vartuli, J.S. Beck, Nature **359**, 710 (1992)
3. T. Yanagisawa, T. Shimizu, K. Kuroda, C. Kato, Bull. Chem. Soc. Jpn. **63**, 988 (1990)
4. S. Hudson, J. Cooney, E. Magner, Angew. Chem. Int. Ed. **47**, 8582 (2008)
5. M. Hartmann, Chem. Mater. **17**, 4577 (2005)
6. A. Takimoto, T. Shiomi, K. Ino, T. Tsunoda, A. Kawai, F. Mizukami, K. Sakaguchi, Micropor. Mesopor. Mater **116**, 601 (2008)
7. E.L. Pires, E.A. Miranda, G.P. Valenca, Appl. Biochem. Biotechnol. **98–100**, 963 (2002)
8. S. Hudson, J. Cooney, B.K. Hodnett, E. Magner, Chem. Mater. **19**, 2049 (2007)
9. C. Montiel, E. Terres, J.M. Dominguez, J. Aburto, J. Mol. Catal. B **48**, 90 (2007)
10. T. Itoh, R. Ishii, T. Hanaoka, Y. Hasegawa, J. Mizuguchi, T. Shiomi, T. Shimomura, A. Yamaguchi, H. Kaneda, N. Teramae, F. Mizukami, J. Mol. Catal. B **57**, 183 (2009)
11. H. Takahashi, B.O. Li, T. Sasaki, C. Miyazaki, T. Kajino, S. Inagaki, Chem. Mater. **12**, 3301 (2000)
12. M.C.R. Hernández, J.E.M. Wejebe, J.C. Basurto, J.I.V. Alcántara, E.T. Rojas, J.T. Ferrara, Int. J. Biol. Macromol. **40**, 444 (2007)
13. Y. Urabe, T. Shiomi, T. Ito, A. Kawai, T. Tsunoda, F. Mizukami, K. Sakaguchi, Chem. Bio. Chem. **8**, 668 (2007)
14. P. Reis, T. Witula, K. Holmberg, Micropor. Mesopor. Mater. **110**, 355 (2007)
15. F.M. Bautista, M.C. Bravo, D. Luna, J.M. Marinas, A.A. Romero, J. Chem. Techol. Biotechnol. **72**, 249 (1998)
16. D. Zhao, Q. Huo, J. Feng, B.F. Chmelka, G.D. Stucky, J. Am. Chem. Soc. **120**, 6024 (1998)
17. F. Kleitz, S.H. Choi, R. Ryoo, Chem. Commun. **17**, 2136 (2003)
18. F. Rouquerol, J. Rouquerol, K. Sing, *Adsorption by Powders and Porous Solids* (Academic Press, London, 1999)
19. J. Lei, J. Fan, C. Yu, L. Zhang, S. Jiang, B. Tu, D. Zhao, Micropor. Mesopor. Mater. **73**, 121 (2004)
20. F.J. Morgan, F.G. Priest, J. Appl. Bacteriol. **50**, 107 (1981)
21. P.H. Pandya, R.V. Jasra, B.L. Newalkar, P.N. Bhatt, Micropor. Mesopor. Mater. **77**, 67 (2005)
22. R. Ravindra, S. Zhao, H. Gies, R. Winter, J. Amer. Chem. Soc. **126**, 12224 (2004)
23. T. Yamamoto, T. Tanaka, T. Funabiki, S. Yoshida, J. Phys. Chem. B **102**, 5830 (1998)
24. T. Kimura, K. Kuroda, Adv. Funct. Mater. **19**, 511 (2009)
25. R.K. Iler, *The Chemistry of Silica* (Wiley, New York, 1979)